Microcalorimetric, reaction kinetics and DFT studies of Pt–Zn/X-zeolite for isobutane dehydrogenation

Joaquin Silvestre-Albero [a], Marco A. Sanchez-Castillo [b], Rong He [b], Antonio Sepúlveda-Escribano [a], Francisco Rodríguez-Reinoso [a] and J.A. Dumesic [b,*]

[a] *Departamento de Química Inorgánica, Universidad de Alicante, Apartado 99, E-03080 Alicante, Spain*
[b] *Department of Chemical Engineering, University of Wisconsin-Madison, Madison, WI 53706, USA*

Received 9 February 2001; accepted 26 March 2001

Microcalorimetric measurements of the adsorption of H_2 and C_2H_4 were carried out at 300 K on a Pt–Zn/X-zeolite catalyst (Pt : Zn atomic ratio equal to 1 : 1). The initial heats of H_2 and C_2H_4 adsorption were equal to 75 and 122 kJ/mol, respectively, and these values are weaker than the values of 90 and 155 kJ/mol typically observed for supported Pt catalysts. Reaction kinetics measurements for isobutane dehydrogenation over the Pt–Zn/X-zeolite catalyst were carried out at temperatures from 673 to 773 K, at isobutane pressures from 0.01 to 0.04 atm, and at hydrogen pressures from 0.1 to 0.7 atm. The catalyst shows high activity and selectivity for dehydrogenation of isobutane to isobutylene. The reaction kinetics can be described with a Horiuti–Polanyi reaction scheme. DFT calculations were carried out for the adsorption of ethylene on slabs of Pt(111), Pt_3Zn(111) and PtZn(011). Results from these calculations indicate that addition of Zn to Pt weakens the binding energies of π-bonded ethylene, di-σ-bonded ethylene, and ethylidyne species on atop, bridged, and three-fold Pt sites, respectively. These effects are most significant for the bonding of ethylidyne species, and they are least significant for π-bonded ethylene species. Results from DFT calculations for the adsorption of formaldehyde show that addition of Zn to Pt weakens the di-σ-bonding at Pt–Pt sites; however, this weakening effect of Zn on formaldehyde adsorption is less significant than the effect on ethylene adsorption. Moreover, the preferred location for adsorption of formaldehyde on PtZn(011) is a Pt–Zn site, whereas the preferred location for adsorption of ethylene is a Pt–Pt site. Thus, formaldehyde is adsorbed more strongly by 53 kJ/mol on PtZn(011) compared to the di-σ-adsorption of ethylene, whereas formaldehyde and ethylene adsorb in the di-σ-forms with comparable energies on Pt(111). This preferred adsorption of formaldehyde compared to ethylene on PtZn(011) may be at least partially responsible for the enhanced selectivity of Pt–Zn-based catalysts for hydrogenation of C=O groups compared to C=C bonds in α,β-unsaturated aldehydes.

KEY WORDS: Pt–Zn/X-zeolite; isobutane dehydrogenation; microcalorimetry; density functional theory

1. Introduction

The addition of Zn to supported platinum catalysts is currently used to control the selectivity of various catalytic processes. For example, the addition of Zn to Pt/Al_2O_3 catalysts promotes the selective reduction of NO [1] and improves the resistance of these systems in waste gas treatment processes [2]. Catalysts based on Pt–Zn supported on ZSM-5 are effective for the conversion of propane to aromatic hydrocarbons [3], and Pt–Zn supported in L-zeolite is used for the selective dehydrogenation of alkanes [4]. Also, mordenite-supported Pt–Zn catalysts are used for dehydroisomerization of *n*-butane to isobutane [5].

Platinum–tin-based catalysts are also widely used in alkane dehydrogenation processes [6]. For example, alumina-supported Pt–Sn catalysts have been used for the dehydrogenation of *n*-decane [7], isobutane [8–11], *n*-butane [12, 13] and propane [8,14–19]. The use of silica-supported Pt–Sn catalysts for the selective dehydrogenation of isobutane has also been reported [8,9,20–32]. Additional studies suggest that Pt–Sn/L-zeolite and Pt–Sn/K-L-zeolite catalysts exhibit high activity and selectivity for isobutane dehydrogenation and high resistance to deactivation [22,23,28,32]. The addition of tin to Pt supported on $ZnAl_2O_4$ has been used to improve the activity and selectivity in isobutane dehydrogenation [33,34]. In this context, it has been reported that Pt/ZnO catalysts can achieve 99% selectivity at 45% conversion in the dehydrogenation of isobutane to isobutylene at 723 K [35].

Another interesting class of reactions for which platinum catalysts modified with tin or zinc have shown good applicability is the selective hydrogenation of α,β-unsaturated aldehydes [36]. The hydrogenation of these compounds can lead to the saturated aldehyde through the hydrogenation of the C=C bond, to the unsaturated alcohol by hydrogenation of the C=O group, or to the saturated alcohol if total hydrogenation takes place. The production of the unsaturated alcohol is generally difficult, since hydrogenation of the C=C group is favored thermodynamically and kinetically [37]. Silica-supported Pt–Sn is one of the most studied catalytic systems for such selective hydrogenation processes. For example, Pt–Sn catalysts have been used for the gas-phase hydrogenation of acrolein [38,39], hydrogenation of crotonaldehyde in either the vapor phase [38,40–43] or liquid phase [40,41,44,45], and liquid-phase hydrogenation of 3-methylcrotonaldehyde, methacrolein and methyl vinyl ketone [38]. In a study of the vapor-phase hydrogenation of crotonaldehyde over Pt–Sn catalysts supported on activated

* To whom correspondence should be addressed.

1011-372X/01/0600-0017$19.50/0

carbon, Coloma *et al.* [46,47] have shown that the catalytic activity and selectivity depended on the Pt/Sn atomic ratio and on the preparation method used, which determined the surface chemical composition of the catalysts and the extent of tin reduction, with the possible formation of Pt–Sn alloy phases. It appears that Zn may have similar effects as Sn for the modification of Pt catalysts in selective hydrogenation processes. Specifically, Consonni *et al.* [48] suggested the use of Pt/ZnO catalysts for the selective vapor-phase hydrogenation of crotonaldehyde, where selectivity to crotyl alcohol (the unsaturated alcohol) increased with the extent of Pt–Zn alloy formation.

In general, the selective dehydrogenation of alkanes over modified Pt catalysts is achieved by the suppression of isomerization and hydrogenolysis, whereas the selective hydrogenation of α,β-unsaturated aldehydes involves the preferential hydrogenation of a C=O group over a C=C group in the same molecule. The addition to Pt of such promoters as Sn leads to the formation of Pt–Sn alloy particles, which reduces the size of surface Pt ensembles and inhibits the formation of highly dehydrogenated surface species required for isomerization, hydrogenolysis and coking reactions [16,20,26,32]. Moreover, the addition of promoters presumably alters the relative accessibility and chemical bond strengths of the C=C and C=O groups to the active species on the catalyst surface [38,49].

Several studies have been conducted to characterize the properties of Pt and Pt–Sn catalysts in terms of structure and adsorption behavior [50–55]. Also, modification of the chemical properties of Pt by Zn has been studied on Zn/Pt(111) surface alloys [56]. It is thus appropriate to compare the catalytic performance of supported Pt–Zn catalysts with respect to supported Pt–Sn catalysts. Such a comparison would provide information about possible differences in the effects caused by the addition of these promoters to Pt, and it would help to address the potential of materials based on Pt–Zn for the selective dehydrogenation of alkanes and for the selective hydrogenation of unsaturated aldehydes. Accordingly, a Pt–Zn/X-zeolite catalyst has been synthesized and studied for isobutane dehydrogenation. In addition, microcalorimetric studies of the adsorption of hydrogen and ethylene were conducted to determine the number of surface sites and to probe the interaction of these molecules with the surface sites. Density functional theory (DFT) calculations were also carried out to investigate the electronic effects of adding Zn on Pt, using ethylene and formaldehyde as probe molecules to study their interactions with Pt(111), Pt_3Zn(111) and PtZn(011) surfaces. These effects of adding Zn to Pt will then be compared to previously reported effects of adding Sn to Pt.

2. Experimental

2.1. Catalyst preparation

The Pt–Zn/X-zeolite catalyst was prepared by sequential addition of Zn and Pt, using a 13X-zeolite (Aldrich) support. The surface area of the zeolite was 520 m^2/g and the pore volume was 0.25 cm^3/g. The 13X-zeolite was loaded with Zn by ion-exchange, using an aqueous solution of $Zn(NO_3)_2{\cdot}6H_2O$ (Aldrich). A ratio of 10 cm^3 of impregnating solution per gram of support was used. The exchange took place during 24 h at room temperature and under continuous agitation. The zeolite was dried overnight at 393 K and treated in air for 4 h at 673 K. The Zn/X-zeolite sample was then impregnated with Pt by evaporative impregnation using an aqueous solution of $H_2PtCl_6{\cdot}6H_2O$ (Aldrich) with a ratio of 10 cm^3 of impregnating solution per gram of support. The excess solvent was removed at 333 K by flowing nitrogen through the suspension, and the remaining solid was dried overnight at 393 K. The resulting Pt–Zn/X-zeolite catalyst contained 0.69 wt% Pt and 0.23 wt% Zn (analyzed by Galbraith Laboratories), corresponding to an atomic ratio of Pt : Zn equal to 1 : 1. The Pt–Zn/X-zeolite catalyst was reduced at 773 K in flowing hydrogen for 10 h prior to further studies.

2.2. Microcalorimetry

Microcalorimetric measurements were performed at room temperature using a Setaram BT2.15D heat-flux calorimeter. Details of the procedures for microcalorimetric measurements can be found elsewhere [57,58]. In short, each sample was treated first in flowing hydrogen at 773 K, followed by treatment in flowing helium for 2 h. Both gases were of ultrahigh purity. The sample was then sealed in a Pyrex capsule, and the capsule was loaded into a set of calorimetric cells [58]. After the sample has reached thermal equilibrium with the calorimeter, the capsule was broken and microcalorimetric measurements were taken by sequentially introducing small doses (*ca.* 1 μmol) of probe molecules onto the sample. The heat signal was recorded as a function of time, and this signal was integrated to obtain the energy released per dose. Volumetric measurements were made to determine the amount of gas adsorbed during the dose, using the dosing pressure, equilibrium pressure, system volumes, and temperature.

The maximum apparent leak rate of the calorimetric cells and the gas handling system, measured by a Baratron capacitance manometer ($\pm 0.5 \times 10^{-4}$ Torr), was 10^{-6} Torr/min in a system volume of $\sim$70 cm^3 (*i.e.,* 10^{-6} μmol/min). The contamination over a typical run ($\sim$5 h) is less than 10^{-3} μmol, which is low compared with the total uptake of sample (*ca.* 1.5 μmol).

2.3. Isobutane dehydrogenation reaction kinetics studies

Reaction kinetics studies of isobutane dehydrogenation on the Pt–Zn/X-zeolite catalyst were carried out using a stainless-steel apparatus and a quartz, down-flow reactor operating at atmospheric pressure. The Pt–Zn/X-zeolite catalyst was mixed with zeolite at a dilution ratio equal to 13.5. All experiments were conducted using approximately 100 mg of the catalyst mixture at a total gas flow rate of

276 cm^3(NTP)/min. Prior to the collection of reaction kinetics data, the catalyst was reduced with hydrogen at 773 K for 10 h and then cooled to the reaction temperature. The feed to the reactor consisted of controlled molar ratios of hydrogen (Liquid Carbonic) and isobutane (AGA, 99.5%). Helium was employed as a carrier gas and it was purified by flowing through activated molecular sieves at 77 K. Hydrogen was purified by flowing through a Deoxo Unit (Engelhard), followed by a bed of molecular sieves at 77 K. Isobutane was used without further purification.

Reaction kinetics studies were carried out at a total pressure of 1 atm and at temperatures of 673, 723 and 773 K. The effect of the isobutane pressure was determined at constant hydrogen initial pressure of 0.1 atm by varying the isobutane feed level between 0.01 and 0.04 atm. The effect of the hydrogen pressure was determined from experiments in which the hydrogen feed level was varied between 0.1 and 0.7 atm, while keeping the isobutane feed level at 0.01, 0.02 and 0.04 atm. The inlet and effluent gas streams from the reactor were analyzed by a HP 5890 gas chomatograph, equipped with a flame-ionization detector. A 15% squalene Chromosorb PAW column (3 m length) was used for gas separation and it was operated isothermally at 303 K.

The fractional conversion of isobutane to isobutene on the Pt–Zn/zeolite catalyst was maintained lower than 45% of the expected equilibrium conversion. For example, at 673 K with a feed composition of 0.01 atm isobutane and 0.7 atm hydrogen, the expected equilibrium conversion was 0.99%, and the observed isobutane conversion was 0.45%. Similarly, at 773 K with a feed composition of 0.04 atm isobutane and 0.1 atm hydrogen, the expected equilibrium conversion was 50.1%, and the observed isobutane conversion was 8.3%. The isobutane dehydrogenation selectivity was 100% at the lower conversion levels of this study and higher than 95% at the higher conversion level. Experiments on the X-zeolite support prior to addition of Pt and Zn indicated that the blank support did not lead to measurable conversion of isobutane under the conditions of the present study.

2.4. DFT calculations

Self-consistent, gradient-corrected, DFT calculations were carried out to investigate the electronic effects of adding zinc to Pt for the adsorption of C_2H_4, CH_2O and H atoms. In this study, we used three layer slabs of Pt(111), Pt_3Zn(111) and PtZn(011), periodically repeated in a super cell geometry with four equivalent layers of vacuum between successive metal slabs. A 2×2 unit cell was used in all calculations, corresponding to $1/4$ monolayer coverage. The structures of the Pt(111) and Pt_3Zn(111) slabs are shown in figure 1(a) (for Pt_3Zn, the black atom represents Zn), and the geometry of the PtZn(011) slab is shown in figure 1(b). Adsorption occurs on one side of the slab to avoid errors originating from the interactions of adsorbates through the slab. In all cases, the top layer and the adsorbate species were allowed to relax, while the bottom two layers are fixed at their bulk positions.

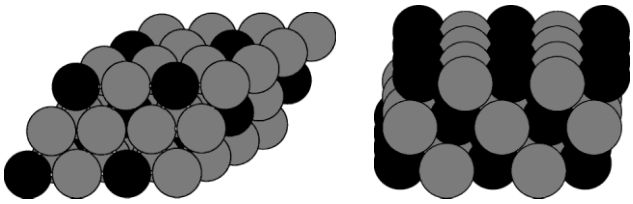

Figure 1. Models of (a) Pt_3Zn(111) and (b) PtZn(011) slabs.

The equilibrium lattice constant determined from DFT calculations for Pt is 4.00 Å [59]. The calculated equilibrium lattice constant for Pt_3Zn is 3.96 Å, and the experimental value is 3.89 Å [60]. The equilibrium lattice constant of the tetragonal PtZn unit cell was determined by fixing the axial ratio c/a at the experimental value (1.223), and then minimizing the electronic energy by varying the lattice constant. The calculated value of the lattice constant is 2.89 Å, and the corresponding experimental value is 2.86 Å [61].

DFT calculations were performed using the Dacapo program, developed at the Danish Technical University [62]. In all calculations, ultrasoft pseudopotentials [63] are used to describe ionic cores, and the Kohn–Sham one-electron valence states are expanded in a basis of plane waves with kinetic energies below 25 Ry. The exchange–correlation energy and potential are described by generalized gradient approximation (PW-91) [64,65]. We have used the non-spin polarized version of the exchange–correlation functional. The surface Brillouin zone is sampled at 18 special k-points.

3. Results and discussion

3.1. Microcalorimetry

Figure 2 shows a plot of differential heat versus adsorbate coverage for hydrogen adsorption on the Pt–Zn/X-zeolite catalyst. The initial heat was 75 kJ/mol, which is comparable with the values of 85 kJ/mol on a $3Pt/Sn/SiO_2$ catalyst and 65 kJ/mol on $Pt/2Sn/SiO_2$; however, this value of 75 kJ/mol is lower than the value of 94 kJ/mol on a Pt/SiO_2

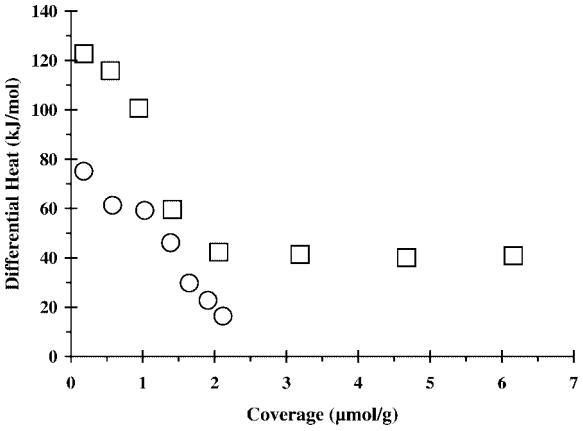

Figure 2. Differential heat *versus* adsorbate coverage for H_2 adsorption (○) and C_2H_4 adsorption (□) on 0.69 wt% Pt/0.23 wt% Zn/X-zeolite at 300 K.

catalyst with similar loading (1.2 wt%) [51]. The saturation uptake of hydrogen was 2.1 μmol/g, which is smaller than the theoretical uptake of approximately 18 μmol/g, assuming 100% dispersion of Pt. As shown below in this paper, results from DFT calculations indicate that the heats of hydrogen adsorption on atop and bridge sites of Pt(111) are –87 and –83 kJ/mol, respectively. The corresponding values for the heats of hydrogen adsorption on atop and bridge sites of PtZn(011) are –61 and −76 kJ/mol, respectively. Therefore, the low uptake of hydrogen on the Pt–Zn/X-zeolite catalyst is most likely caused either by significant enrichment of the surface with Zn, or by inhibition of the rate of hydrogen dissociation upon addition of Zn to Pt. In this latter respect, a similar large inhibition of hydrogen adsorption was observed on Sn/Pt(111) surface alloys [66], on unsupported Pt–Sn polycrystalline alloys [67] and on supported Pt–Sn alloy catalysts [68], and it was shown that the inhibition of H_2 adsorption on the Sn/Pt(111) surface alloy was caused by a kinetic effect [66].

The results of ethylene adsorption on the Pt–Zn/X-zeolite catalyst at room temperature are also shown in figure 2. Ethylene adsorption on this catalyst gave an initial heat of 122 kJ/mol, which is comparable with the value of 115 kJ/mol for a $Pt/Sn/SiO_2$ catalyst with a Pt : Sn atomic ratio of 1 : 1.5 and having a similar Pt loading (1.2 wt%) [20]. Initial heats of ethylene adsorption on $3Pt/Sn/SiO_2$ and $Pt/2Sn/SiO_2$ catalysts were measured to be 129 and 94 kJ/mol, respectively [51]. In general, the dissociative adsorption of ethylene on Pt to give ethylidyne species and adsorbed atomic hydrogen leads to a heat of approximately 155 kJ/mol [20]; therefore, the lower heat of 122 kJ/mol measured on the Pt–Zn/X-zeolite catalyst suggests that most of the ethylene is adsorbed in the molecular state (*i.e.*, as π-adsorbed or di-σ-adsorbed ethylene species).

Figure 2 also shows a plateau near 40 kJ/mol for ethylene adsorption on the Pt–Zn/X-zeolite catalyst. The isosteric heat of ethylene adsorption for X-zeolite has been measured to be 37 kJ/mol [69], which is the same value as determined for the desorption of ethylene from X-zeolite [70]. As shown below in this paper, results from our DFT calculations indicate that the energy changes for adsorption of ethylene on PtZn(011) to form π-bonded ethylene and di-σ-bonded ethylene are both equal to −41 kJ/mol. Therefore, the plateau in figure 2 at ∼40 kJ/mol for the heat of ethylene adsorption is likely to be caused from adsorption on both the PtZn alloy and the X-zeolite support.

3.2. Isobutane dehydrogenation reaction kinetics studies

The rate of isobutane dehydrogenation was calculated as a turnover frequency (TOF) based on the saturation uptake of H_2 on the catalyst obtained from our calorimetric measurements (*i.e.*, 4.2 μmol of sites per gram). Figure 3 shows the dependence of the TOF with respect to the inlet isobutane pressure at temperatures of 673, 723 and 773 K. These data were collected at a constant hydrogen pressure of 0.1 atm. For each temperature, the inlet isobutane pressure was varied between 0.01 and 0.04 atm. The kinetic orders of isobutane dehydrogenation with respect to the isobutane pressure were 0.88, 0.76 and 0.80, for the experiments at 673, 723 and 773 K, respectively.

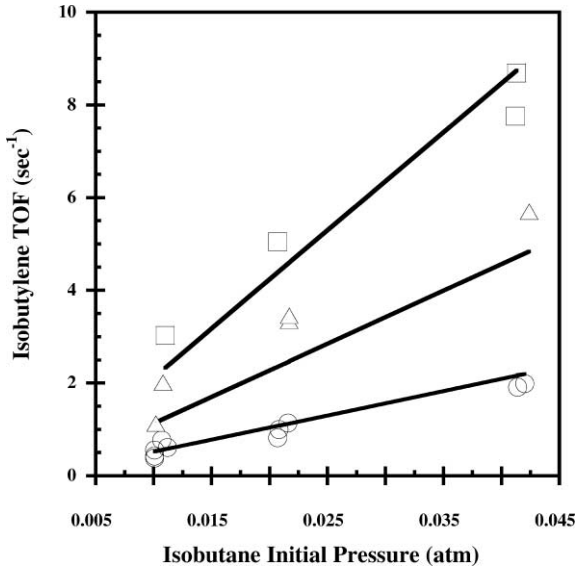

Figure 3. Isobutylene TOF as a function of isobutane initial pressure at (○) 673, (△) 723 and (□) 773 K. The kinetic data were collected at hydrogen initial pressure 0.1 atm. Solid lines correspond to predictions of the kinetic model.

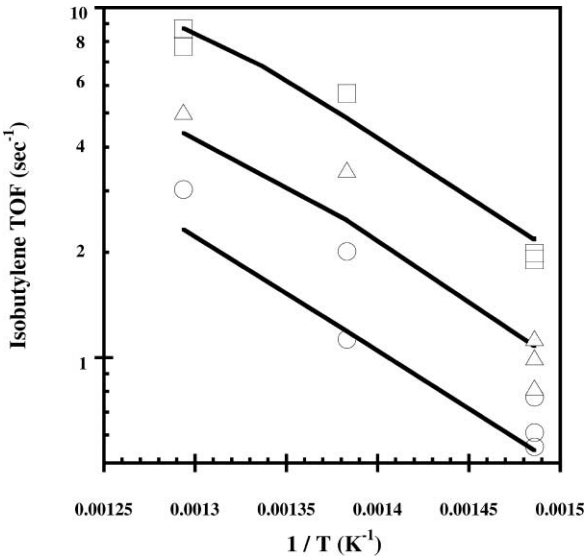

Figure 4. Isobutylene TOF as a function of temperature at different isobutane feed pressure: (○) 0.01, (△) 0.02 and (□) 0.04 atm. The kinetic data were collected at hydrogen initial pressure 0.1 atm. Solid lines correspond to predictions of the kinetic model.

Figure 4 shows the effect of temperature on the TOF at isobutane inlet pressures of 0.01, 0.02 and 0.04 atm, while keeping the hydrogen pressure at 0.1 atm. The apparent activation energies of isobutane dehydrogenation at these reaction conditions were 61.2, 72.7 and 76.4 kJ/mol, respectively. The apparent activation energies are lower than the overall enthalpy change of the isobutane dehydrogenation reaction (122.5 kJ/mol at 723 K).

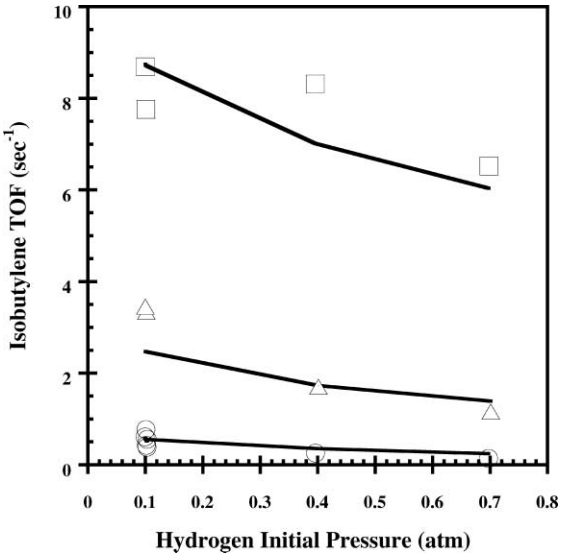

Figure 5. Isobutylene TOF as a function of hydrogen initial pressure at (○) 673 K and 0.01 atm of isobutane in the feed, (△) 723 K and 0.02 atm of isobutane in the feed and (□) 773 K and 0.04 atm of isobutane in the feed. Solid lines correspond to predictions of the kinetic model.

Figure 5 shows the effect of the hydrogen pressure on the TOF at various temperatures and isobutane feed pressures. There different cases are shown: 0.01 atm of isobutane and 673 K, 0.02 atm of isobutane and 723 K, and 0.04 atm of isobutane and 773 K. The kinetic orders of isobutane dehydrogenation with respect to hydrogen pressure were −0.86, −0.55 and −0.06, respectively.

Cortright and Dumesic [28] conducted kinetic studies of isobutane dehydrogenation over a Pt–Sn/L-zeolite catalyst, under the same temperature range and similar isobutane and hydrogen pressures used in the present study. The kinetic orders with respect to isobutane were 0.8, 0.8 and 0.9 at 673, 723 and 773 K, respectively. Our results are in close agreement with these values. Similarly, the kinetic order with respect to hydrogen at 673 K was −0.6 over the Pt–Sn/L-zeolite catalyst, which is also in good agreement with the results of the present study.

3.3. DFT calculations

Figure 6 shows the primary adsorbed configurations of C_2H_4 on $Pt_3Zn(111)$. These species are π-bonded ethylene, di-σ-bonded ethylene, and ethylidyne species, occurring on atop, bridge, hcp-hollow and fcc-hollow three-fold sites, respectively. Figure 7 shows the geometries for π-bonded and di-σ-bonded ethylene on PtZn(011). We note that three-fold sites for the adsorption of ethylidyne species are not present on the PtZn(011) surface. Figure 8 shows the geometries for di-σ-bonded formaldehyde on Pt(111), $Pt_3Zn(111)$ and PtZn(011). The formation of di-σ-bonded formaldehyde occurs on bridge sites formed by two Pt atoms on Pt(111), and on bridge sites formed by two Pt atoms or a Pt atom and an adjacent Zn atom on $Pt_3Zn(111)$ and PtZn(011), with the oxygen atom oriented toward the Zn atom.

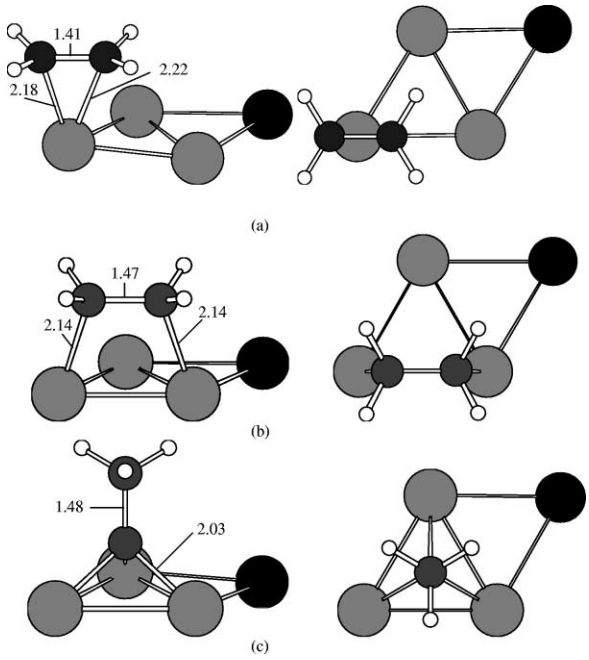

Figure 6. Side and top views for adsorption of (a) π-bonded ethylene on atop site, (b) di-σ-bonded ethylene on bridge site and (c) ethylidyne species on three-fold site on $Pt_3Zn(111)$. Bond lengths are in angstroms.

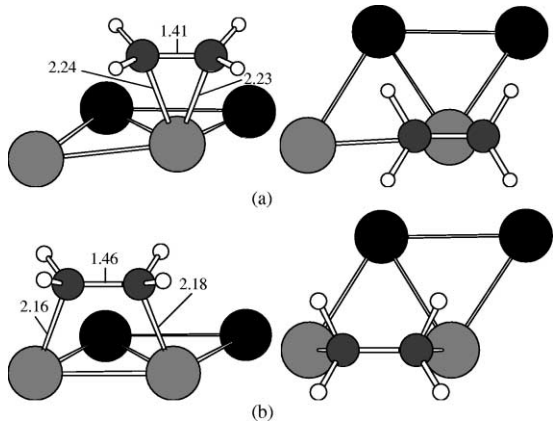

Figure 7. Side and top views for adsorption of (a) π-bonded ethylene on atop site and (b) di-σ-bonded ethylene on bridge site on PtZn(011). Bond lengths are in angstroms.

Calculated energy changes for adsorption of C_2H_4 on $Pt_3Zn(111)$ and PtZn(011) are listed in table 1. For comparison, this table also shows calculated values of energy changes for C_2H_4 adsorption on Pt(111) and $Pt_3Sn(111)$ [71,72]. The energy changes for forming π-bonded ethylene, di-σ-bonded ethylene and ethylidyne species on Pt(111) are −73, −117 and −95 kJ/mol (hcp and fcc sites), respectively. The corresponding values on $Pt_3Zn(111)$ are −64, −98, −99 (on hcp sites) and −77 kJ/mol (on fcc sites), respectively. Therefore, π-bonded species and di-σ-bonded ethylene species are bonded more weakly on $Pt_3Zn(111)$ than on Pt(111) by 9 and 19 kJ/mol, respectively. In contrast, π-bonded species and di-σ-bonded ethylene species are bonded more weakly by 21 and 31 kJ/mol, respectively, on $Pt_3Sn(111)$ compared to Pt(111). Thus the electronic ef-

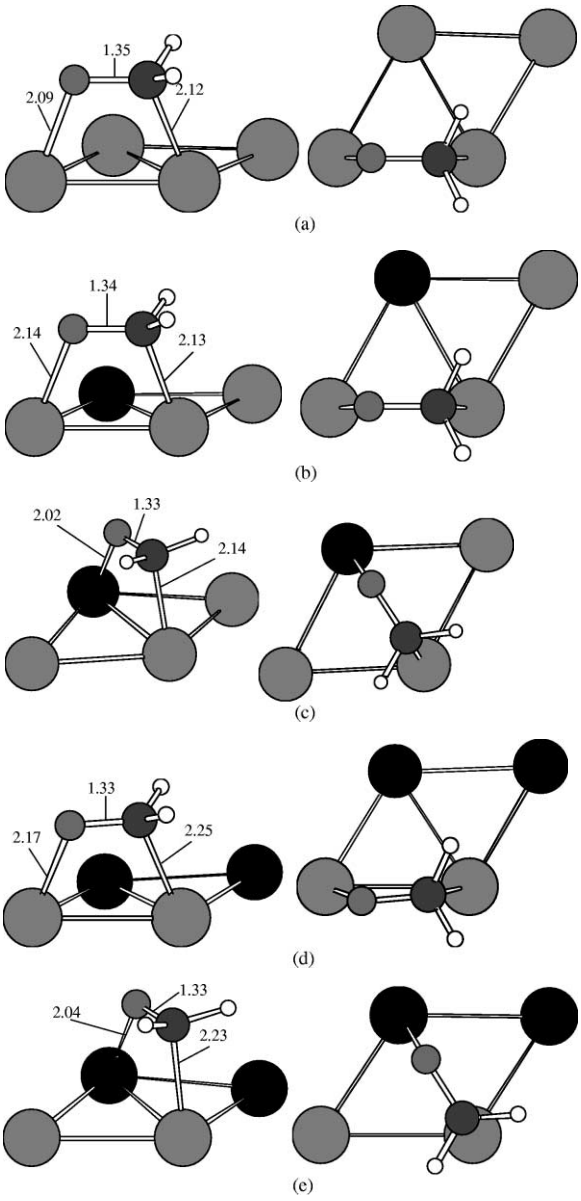

Figure 8. Side and top views for adsorption of formaldehyde on (a) bridge site of Pt(111), (b) Pt–Pt bridge site on $Pt_3Zn(111)$, (c) Pt–Zn bridge site on $Pt_3Zn(111)$, (d) Pt–Pt bridge site on PtZn(011), and (e) Pt–Zn bridge site on PtZn(011). Bond lengths are in angstroms.

fect of Zn is not as strong as for Sn, though similar weakening trends with respect to atop and bridge sites are observed. Calculations on the PtZn(011) slab show that the higher concentration of Zn lowers the energy changes for forming π-bonded and di-σ-bonded ethylene to the same value of -41 kJ/mol.

Bonding of ethylidyne species on fcc sites of $Pt_3Zn(111)$ is weaker than on Pt(111) by 18 kJ/mol, whereas energy changes for bonding these species on hcp sites are similar on $Pt_3Zn(111)$ and Pt(111). These results for the adsorption of ethylidyne species on $Pt_3Zn(111)$ differ from results on $Pt_3Sn(111)$, where significant weakening of the bonding at three-fold sites is observed (*i.e.*, weaker bonding by 84 and 50 kJ/mol on hcp and fcc sites, respectively).

Selected bond lengths are shown in figures 6 and 7 for various adsorbates on the $Pt_3Zn(111)$ and PtZn(011) slabs. Lengths of C–Pt and C–C bonds for these adsorbates are compared in table 2 with values calculated on Pt(111) and $Pt_3Sn(111)$ slabs. For a given adsorbate, the C–Pt bond becomes elongated as the interaction with surface becomes weaker. The C–C bond lengths for di-σ-bonded ethylene on $Pt_3Zn(111)$ and $Pt_3Sn(111)$ are both 1.47 Å, and the value on PtZn(011) is 1.46 Å; these values are slightly shorter than the value of 1.48 Å on Pt(111).

The energy changes for adsorption of formaldehyde to form di-σ-bonded species on Pt–Pt bridge sites of Pt(111), $Pt_3Zn(111)$ and PtZn(011) are -122, -124 and -83 kJ/mol, respectively. Thus, whereas addition of Zn to Pt weakens the bonding of di-σ-bonded ethylene species by 76 kJ/mol on PtZn(011), the di-σ-bonded formaldehyde species are weakened by only 39 kJ/mol. The energy changes for adsorption of formaldehyde to form di-σ-bonded species on Pt–Zn sites of $Pt_3Zn(111)$ and PtZn(011) are -97 and -94 kJ/mol. Accordingly, the Pt–Pt bridge sites are preferred by 27 kJ/mol for adsorption of formaldehyde on $Pt_3Zn(111)$, whereas the Pt–Zn bridge sites are preferred by 11 kJ/mol on PtZn(011). Given that formaldehyde adsorption is preferred on the Pt–Zn site of PtZn(011), addition of Zn to Pt now weakens the bonding of di-σ-bonded formaldehyde species by only 27 kJ/mol compared to Pt(111), which is significantly smaller than the extent of weakening for adsorption of di-σ-bonded ethylene species

Table 1
Results from DFT calculations for changes in electronic energies (kJ/mol) for interaction of adsorbates with Pt(111)[a], $Pt_3Zn(111)$, $Pt_3Sn(111)$[a] and PtZn(011) slabs.

Reaction[b]	Pt(111)	$Pt_3Zn(111)$	$Pt_3Sn(111)$	PtZn(011)
$C_2H_4 + * \rightleftharpoons *C_2H_4$ (π)	-73	-64	-52	-41
$C_2H_4 + * \rightleftharpoons *C_2H_4$ (di-σ)	-117	-98	-86	-41
$C_2H_4 + * \rightleftharpoons *CCH_3$ (hcp) $+ \frac{1}{2}H_2$	-95	-99	-11	
$C_2H_4 + * \rightleftharpoons *CCH_3$ (fcc) $+ \frac{1}{2}H_2$	-95	-77	-45	
$CH_2O + * \rightleftharpoons *CH_2O$ (Pt–Pt bridge sites)	-122	-124		-83
$CH_2O + * \rightleftharpoons *CH_2O$ (Pt–Zn bridge sites)		-97		-94
$H_2 + 2* \rightleftharpoons 2*H$ (atop sites)	-87[c]			-61
$H_2 + 2* \rightleftharpoons 2*H$ (bridge sites)	-83[c]			-76

[a] [71].
[b] $*$ denotes the metal surface.
[c] [72].

Table 2
Bond lengths (Å) from DFT calculations for interaction of C_2H_4 with Pt(111)[a], $Pt_3Zn(111)$, $Pt_3Sn(111)$[a] and PtZn(011) slabs.

Bond	Slab	C_2H_4 (π)	C_2H_4 (di-σ)	CCH_3[b] (ethylidyne)
	Pt(111)	2.18	2.11	2.02
C–Pt	$Pt_3Zn(111)$	2.18, 2.22	2.14	2.03
	$Pt_3Sn(111)$	2.21	2.15	2.05
	PtZn(011)	2.23, 2.24	2.16, 2.18	
	Pt(111)	1.41	1.48	1.49
C–C	$Pt_3Zn(111)$	1.41	1.47	1.48
	$Pt_3Sn(111)$	1.40	1.47	1.47
	PtZn(011)	1.41	1.46	

[a] [71].
[b] On hcp sites.

Table 3
Bond lengths (Å) from DFT calculations for interaction of CH_2O with Pt(111), $Pt_3Zn(111)$ and PtZn(011) slabs.

	Pt(111)	$Pt_3Zn(111)$		PtZn(011)	
	Pt–Pt site	Pt–Pt site	Pt–Zn site	Pt–Pt site	Pt–Zn site
C–O	1.35	1.34	1.33	1.33	1.33
Pt–O	2.09	2.14		2.17	
Zn–O			2.02		2.04
Pt–C	2.12	2.13	2.14	2.25	2.23

(76 kJ/mol). This trend in adsorption behavior is consistent with the suggestion that crotonaldehyde adsorbs by the carbonyl group rather than by the C=C double bond during selective hydrogenation of crotonaldehyde on Pt/ZnO catalysts [48].

Lengths of C–O, Pt–O, Zn–O and Pt–C bonds are listed in table 3 for di-σ-bonded formaldehyde species on Pt(111), $Pt_3Zn(111)$ and PtZn(011). The distances of C–O bond range from 1.33 to 1.35, which is considerably longer than the length of a normal double bond in a carbonyl group (1.2 Å). The variations of Pt–O, Zn–O and Pt–C bond distances show trends with respect to binding energy. For example, as Zn is added to Pt, the C–O length decreases, the Pt–O length increases, and the Pt–C length increases. In general, Zn–O bonds are shorter than Pt–O bonds. Lastly, the C–O bond is tilted 6.4° and 8.5° relative to the surface plane for di-σ-bonded formaldehyde species on $Pt_3Zn(111)$ and PtZn(011), respectively.

Finally, table 1 shows values of the energy changes for dissociative adsorption of H_2 on Pt(111) and PtZn(011). These values are equal to −87 and −83 kJ/mol on Pt(111) to form H atoms at atop sites and bridge-bonded sites, respectively, whereas the corresponding values are equal to −61 and −76 kJ/mol on PtZn(011). We note that the energy change for dissociative adsorption of H_2 on Pt(111) to form H atoms at three-fold sites is equal to –88 kJ/mol, and these sites are not present on PtZn(011).

3.4. Analysis of reaction kinetics for isobutane dehydrogenation

The results from our reaction kinetics studies of isobutane dehydrogenation can be combined with results from microcalorimetric measurements and DFT calculations to describe the surface chemistry in terms of a Horiuti–Polanyi mechanism shown below [23,28]:

$$C_4H_{10} + 2* \rightarrow C_4H_9* + H* \quad (1)$$

$$C_4H_9* + 2* \rightarrow C_4H_8** + H* \quad (2)$$

$$C_4H_8** \rightarrow C_4H_8 + 2* \quad (3)$$

$$H_2 + 2* \rightarrow 2H* \quad (4)$$

The dissociative adsorption of isobutane has been shown for Pt–Sn-based catalysts to be the rate-determining step in this mechanism [23]. Accordingly, we have assumed that steps (2)–(4) are quasi-equilibrated for the experimental conditions of this study, and the following rate expression can be used to describe the kinetics of the dehydrogenation process:

$$r_{DH} = k_1\theta_*^2\left[P_{iC_4H_{10}} - \frac{P_{iC_4H_8}P_{H_2}}{K_{eq}}\right], \quad (5)$$

where r_{DH} is the net dehydrogenation rate, k_1 is the rate constant for the dissociative adsorption of isobutane, K_{eq} is the overall equilibrium constant for isobutane dehydrogenation and θ_* is the fraction of sites free of adsorbed species. Cortright *et al.* [23] reported that the fractional coverage of isobutyl species is very small under similar reaction conditions for a 0.5 wt% Pt–Sn/L-zeolite (Pt : Sn = 1 : 2.5); therefore, the value of θ_* is dependent on the adsorption–desorption quasi-equilibria of steps (3) and (4), as given by

$$\theta_* = \frac{-K_3}{4P_{iC_4H_8}}\left[1 + \sqrt{K_4P_{H_2}} - \sqrt{1 + \sqrt{K_4P_{H_2}} + K_4P_{H_2} + \frac{8P_{iC_4H_8}}{K_3}}\right], \quad (6)$$

where K_3 is the equilibrium constant for isobutene desorption and K_4 is the equilibrium constant for hydrogen adsorption.

As seen in equations (5) and (6), the rate of isobutane dehydrogenation depends on the values of k_1, K_3, and K_4 (as well as the known value of K_{eq}). These kinetic parameters can be described in terms of physically meaningful quantities such as standard entropies and enthalpy changes. The standard entropy changes were expressed in terms of known entropies for gaseous species, and unknown entropies for adsorbed species and the activated complex for step (1). The standard enthalpy changes were also set as kinetic parameters and were constrained according to the results of microcalorimetric measurements and DFT calculations. Accordingly, a quantitative description of isobutane dehydrogenation can be made in terms of six parameters: $S_1^{\neq}$, S_{H*}, $S_{iC_4H_8*}$, $\Delta H_1^{\neq}$, ΔH_3 and ΔH_4. The values for this set of parameters were determined by using the apparent reaction rate expression (r_{DH}), combined with PFR reactor design equations to fit the experimental results of the kinetic studies.

The kinetic parameters involved with steps (3) and (4) showed low sensitivity for fitting the reaction kinetics data. For this reason, the values of $S_{iC_4H_8*}$, and S_{H*} were set to

Table 4
Fitted kinetic parameters for Pt–Zn/X-zeolite catalyst.[a]

Elementary step	Parameter	Value	95% confidence limit
(1)	$S_1^{\neq}$	299	292–307
Forward activation	$\Delta H_1^{\neq}$	58.6	52.9–64.4
(3)	$S_{i\mathrm{C_4H_8}*}$	262	Fixed
Quasi-equilibrated	ΔH_3	41	Fixed
(4)	$S_{\mathrm{H}*}$	35	Fixed
Quasi-equilibrated	ΔH_4	−50	Fixed

[a] Entropies are given in J/mol K and enthalpy changes in kJ/mol. Standard entropies at 723 K and 1 atm: $S^0_{i\mathrm{C_4H_{10}}} = 421$ J/mol K; $S^0_{i\mathrm{C_4H_8}} = 405$ J/mol K; $S^0_{\mathrm{H_2}} = 157$ J/mol K.

the values reported by Cortright *et al.* [28] for a 0.5 wt% Pt–Sn/L-zeolite catalyst. The value for ΔH_3 was set equal to 41 kJ/mol, as given by the results from DFT calculations; and the value for ΔH_4 was set equal to −50 kJ/mol, as given by the average heat of hydrogen adsorption determined from our microcalorimetric measurements. Table 4 shows the fitted kinetic parameters and their corresponding 95% confidence limit. The value of $S_1^{\neq}$ corresponds to a surface species having between 1° and 2° of translational freedom, which suggests a fairly mobile transition state. The solid lines in figures 3–5 represent the predictions of the model, and it can be seen that the kinetic model provides a good fit of the experimental data.

The value of the rate constant for step (1) at 720 K (the average temperature of the present study) is about five times smaller than the rate constant for a 0.5 wt% Pt–Sn/L-zeolite catalyst [28]. Since both of these rate constants were derived using the same rate expression and using the same method to count sites (*i.e.*, H_2 adsorption), it appears that the Pt–Sn/L-zeolite catalyst is slightly more active than the present Pt–Zn/X-zeolite catalyst. However, this difference is rather small given the difficulty in counting with precision the number of active sites.

4. Conclusions

The Pt–Zn/X-zeolite catalyst of the present study shows high activity and selectivity for the dehydrogenation of isobutane to isobutylene at temperatures from 673 to 773 K. The rate of isobutane dehydrogenation per site counted by H_2 adsorption is comparable (*i.e.*, lower by a factor of ∼5) to the activity of a Pt–Sn/L-zeolite catalyst. Microcalorimetric measurements of the adsorption of H_2 and C_2H_4 on the Pt–Zn/X-zeolite catalyst are similar to results reported in the literature for adsorption on silica-supported Pt–Sn catalysts. Therefore, it appears that effects of adding Zn to Pt are qualitatively similar to the effects of adding Sn to Pt.

Results from DFT calculations for the adsorption of ethylene on slabs of Pt(111), Pt_3Zn(111), Pt_3Sn(111) and PtZn(011) indicate that addition of Zn or Sn to Pt weakens the binding energies of π-bonded ethylene, di-σ-bonded ethylene, and ethylidyne species on atop, bridged, and threefold Pt sites, respectively. These effects are most significant for the bonding of ethylidyne species, and they are least significant for π-bonded ethylene species. Importantly, comparisons of Pt_3Zn(111) and Pt_3Sn(111) slabs indicate that the electronic effects of adding Zn to Pt are less significant than the effects of adding Sn; and, comparisons of Pt_3Zn(111) and PtZn(011) slabs indicate that the electronic effects of adding Zn to Pt are more significant at higher Zn concentrations.

Results from DFT calculations for the adsorption of formaldehyde on slabs of Pt(111), Pt_3Zn(111) and PtZn(011) show that addition of Zn to Pt weakens the di-σ-bonding at Pt–Pt sites; however, this effect of Zn on formaldehyde adsorption is less significant than the effect on ethylene adsorption, *i.e.*, di-σ-adsorbed formaldehyde is weakened by 39 kJ/mol on PtZn(011) compared to Pt(111), whereas di-σ-adsorbed ethylene is weakened by 76 kJ/mol. Comparison of DFT results from Pt_3Zn(111) and PtZn(011) slabs shows that the binding energy of di-σ-adsorbed formaldehyde at Pt–Zn sites is insensitive to the Zn concentration, *i.e.*, the binding energies are equal to 97 and 94 kJ/mol, respectively. Therefore, the preferred location for adsorption of formaldehyde on PtZn(011) is a Pt–Zn site, whereas the preferred location for adsorption of ethylene is a Pt–Pt site. Moreover, the formaldehyde is adsorbed more strongly by 53 kJ/mol on PtZn(011) compared to the di-σ-adsorption of ethylene, whereas formaldehyde and ethylene adsorb in the di-σ-forms with comparable energies on Pt(111). This preferred adsorption of formaldehyde compared to ethylene on PtZn(011) may be at least partially responsible for the enhanced selectivity of Pt–Zn-based catalysts for hydrogenation of C=O groups compared to C=C bonds in α,β-unsaturated aldehydes.

Acknowledgement

We wish to acknowledge funding from the National Science Foundation, which supported studies at the University of Wisconsin. Financial support from CICYT (Spain; project QUI98-0663) is gratefully acknowledged. JSA also acknowledges a grant from University of Alicante. We wish to thank Dr. Randy Cortright for valuable discussions throughout this work. In addition, we thank Professors Jens Nørskov (Danish Technical University) and Manos Mavrikakis (University of Wisconsin) for assistance with the Dacapo software used to conduct DFT slab calculations.

References

[1] A. Bensaddik, N. Mouaddib, M. Krawczyk, V. Pitchon, F. Garin and G. Maire, Stud. Surf. Sci. Catal. 116 (1998) 265.
[2] M. Oshimura, A. Kawakami, S. Fujii, Y. Kori, N. Odani, S. Yamaguchi, H. Hosoda, O. Watanabe, A. Miake and O. Okamoto, JP patent 51054094 (1976).
[3] Z. Hou, R. Cao and D. He, Fenzi Cuihua 12 (1998) 214.
[4] B.D. Alexander and G.A.J. Huff, US patent 5453558 (1995).
[5] M.M. Ramirez-Corredores, T. Romero and M. Gonzalez, Prepr. Am. Chem. Soc. Div. Pet. Chem. 44 (1999) 146.
[6] F. Buonomo, D. Sanfilippo and F. Trifirò, in: *Handbook of Heterogeneous Catalysis*, eds. G. Ertl, H. Knözinger and J. Weitkamp (VCH, Weinheim, 1997) pp. 2140–2151.

[7] G.T. Gokak, A.G. Basrur, D. Rajesward, G.S. Rao and K.R. Krishnamurthy, React. Kinetic. Catal. Lett. 59 (1996) 315.
[8] L.C. Loc, H.S. Thoang, N.A. Gaisai and S.L. Kiperman, Stud. Surf. Sci. Catal. 75 (1993) 2277.
[9] G.J. Siri, M.L. Cassella, G.F. Santori and O.A. Ferreti, Ind. Eng. Chem. Res. 36 (1997) 4821.
[10] G. Corro, P. Marecot and J. Barbier, *Catalyst Deactivation*, Stud. Surf. Sci. Catal., Vol. 111 (Elsevier, Amsterdam, 1997) pp. 359–366.
[11] S. Kogan, M. Herkowitz, H.M. Woerde and P.F.V.D. Oosterkamp, DGNK Tagungsber. 9705 (1997) 117.
[12] L. Wang, L. Lin, T. Zang and H. Cai, React. Kinet. Catal. Lett. 52 (1994) 107.
[13] Z. Xu, Z.T.Y. Fang and L. Lin, Stud. Surf. Sci. Catal. (1997) 425.
[14] M. Larsson, B. Andersson, O.A. Bariaas and A. Holmen, Stud. Surf. Sci. Catal. 88 (1994) 233.
[15] L.V. Babenkova, S. Szabo, I. Naidina and Y.G. Kulievskaya, ACH Models Chem. 131 (1994) 113.
[16] S. De-Miguel, A. Castro, O. Scelze, J.L.G. Fierro and J. Soria, Catal. Lett. 36 (1996) 201.
[17] H.P. Rebo, E.A. Blekkan, L. Bednarova and A. Holmen, *Catalyst Deactivation, 1999*, Stud. Surf. Sci. Catal., Vol. 126 (Elsevier, Amsterdam, 1999) pp. 237–247.
[18] S. Assabumrungrat, W. Jhoraleecharnchai, P. Praserthdam and S. Goto, J. Chem. Eng. Jpn. 33 (2000) 529.
[19] P. Praserthdam, N. Grisdanurak and W. Yuangsawatdikul, Chem. Eng. J. 77 (2000) 215.
[20] R.D. Cortright and J.A. Dumesic, J. Catal. 148 (1994) 771.
[21] R.D. Cortright and J.A. Dumesic, J. Catal 152 (1995) 576.
[22] R.D. Cortright and J.A. Dumesic, Appl. Catal. A 129 (1995) 101.
[23] R.D. Cortright, E. Bergene, P.E. Levin, M.A. Natal-Santiago and J.A. Dumesic, in: *11th Int. Congr. on Catalysis – 40th Anniversary*, Stud. Surf. Sci. Catal., Vol. 101 (Elsevier, Amsterdam, 1996) pp. 1185–1194.
[24] B.E. Spiewak, P.E. Levin, R.D. Cortright and J.A. Dumesic, J. Phys. Chem. 100 (1996) 17260.
[25] S.M. Stagg, C.A. Querini, W.E. Alvarez and D.E. Resasco, J. Catal. 168 (1997) 75.
[26] J.M. Hill, R.D. Cortright and J.A. Dumesic, Appl. Catal. A 168 (1998) 9.
[27] F. Humblot, J.P. Candy, F. LePeltier, B. Didillon and J.M. Basset, J. Catal. 179 (1998) 459.
[28] R.D. Cortright, P.E. Levin and J.A. Dumesic, Ind. Eng. Chem. Res. 37 (1998) 1717.
[29] R.D. Cortright and J.A. Dumesic, US Patent 5736478 (1998).
[30] J. Llorca, N. Homs, J. Leon, J.G. Fierro and P.R.d.l. Piscina, Appl. Catal. A 189 (1999) 77.
[31] J.P. Candy, F. Humblot, B. Didillon, F. LePeltier and J.M. Basset, *Catalyst Deactivation, 1999*, Stud. Surf. Sci. Catal., Vol. 126 (Elsevier, Amsterdam, 1999) pp. 237–247.
[32] R.D. Cortright, J.M. Hill and J.A. Dumesic, Catal. Today 55 (2000) 213.
[33] H. Miura, T. Itoh, M. Ikenishi and T. Tsuchiya, Tagungsber. 9705 (1997) 259.
[34] H. Miura and T. Itoh, React. Kinet. Catal. Lett. 66 (1999) 189.
[35] A. Igarashi and M. Ohta, Sekiyu Gakkaishi 37 (1994) 64.
[36] P. Claus, Topics Catal. 5 (1998) 51.
[37] P.N. Rylander, *Catalytic Hydrogenation in Organic Syntheses* (Academic Press, New York, 1979).
[38] T.B.L.W. Marinelli, S. Nabuurs and V. Ponec, J. Catal. 151 (1995) 431.
[39] T.B.L.W. Marinelli and V. Ponec, J. Catal. 156 (1995) 51.
[40] J.L. Margitfalvi, I. Borbath, E. Tfirst and A. Tompos, Catal. Today 43 (1998) 29.
[41] J.L. Margitfalvi, I. Borbath and A. Tompos, Chem. Ind. 75 (1998) 243.
[42] J.L. Margitfalvi, I. Borbath and A. Tompos, Stud. Surf. Sci. Catal. 118 (1998) 195.
[43] F. Coloma, J. Lorca, N. Homs, P.R.d.l. Piscina, F. Rodríguez-Reinoso and A. Sepúlveda-Escribano, Phys. Chem. Chem. Phys. 2 (2000) 3063.
[44] G.F. Santori, M.L. Casella, G.J. Siri, H.R. Adúriz and O.A. Ferreti, Appl. Catal. A 197 (2000) 141.
[45] J.L. Margitfalvi, G. Vanko, I. Borbath, A. Tompos and A. Vertes, J. Catal. 190 (2000) 474.
[46] F. Coloma, A. Sepúlveda-Escribano, J.L.G. Fierro and F. Rodríguez-Reinoso, Appl. Catal. 136 (1996) 231.
[47] F. Coloma, A. Sepúlveda-Escribano, J.L.G. Fierro and F. Rodríguez-Reinoso, Appl. Catal. 148 (1996) 63.
[48] M. Consonni, D. Jokic, D.Y. Murzin and R. Toroude, J. Catal. 188 (1999) 165.
[49] V. Ponec, Appl. Catal. A 149 (1997) 27.
[50] H. Lieske, A. Sárkány and J. Völter, Appl. Catal. 30 (1987) 69.
[51] J. Shen, J.M. Hill, R.M. Watwe, B.E. Spiewak and J.A. Dumesic, J. Phys. Chem. 103 (1999) 3923.
[52] K. Balakrishnan and J. Schwank, J. Catal. 127 (1991) 287.
[53] T.P. Chojnacki and L.D. Schmidt, J. Catal. 129 (1991) 473.
[54] G. Meitzner, G.H. Via, F.W. Lytle, S.C. Fung and J.H. Sinfelt, J. Phys. Chem. 92 (1988) 2925.
[55] F.B. Passos, M. Schmal and M.A. Vannice, J. Catal. 160 (1996) 106.
[56] J.A. Rodriguez and M. Kuhn, J. Chem. Phys. 102 (1995) 4279.
[57] B.E. Spiewak, J. Shen and J.A. Dumesic, J. Phys. Chem. 99 (1995) 17640.
[58] B.E. Spiewak and J.A. Dumesic, Thermochim. Acta 290 (1997) 43.
[59] R.M. Watwe, R.D. Cortright, J.K. Nørskov and J.A. Dumesic, J. Phys. Chem. B 104 (2000) 2299.
[60] P.M. Hansen, *Constitution of Binary Alloys* (McGraw-Hill, New York, 1958).
[61] H. Nowotny, E. Bauer, A. Stempfl and H. Bittner, Monatsh. Chem. 83 (1952) 221.
[62] B. Hammer, L.B. Hansen and J.K. Nørskov, Phys. Rev. B 59 (1999) 7413.
[63] D. Vanderbilt, Phys. Rev. B 41 (1990) 7892.
[64] J.A. White and D.M. Bird, Phys. Rev. B 50 (1994) 4954.
[65] J.P. Perdew, J.A. Chevary, S.H. Vosko, K.A. Jackson, M.R. Pederson, D.J. Singh and C. Fiolhais, Phys. Rev. B 46 (1992) 6671.
[66] M.T. Paffett, S.C. Gebhard, R.G. Windham and B.E. Koel, J. Phys. Chem. 94 (1990) 6831.
[67] H. Verbeek and W.M.H. Sachtler, J. Catal. 42 (1976) 257.
[68] H. Lieske and J. Völter, J. Catal. 90 (1984) 96.
[69] A.G. Bezus, A.V. Kiselev, Z. Sedlacek and P.Q. Du, J. Chem. Soc. Faraday Trans. 67 (1971) 468.
[70] M. Kiskinova, G.L. Griffin and J.T. Yates, J. Catal. 71 (1981) 278.
[71] R.M. Watwe, R.D. Cortright, M. Mavrikakis, J.K. Nørskov and J.A. Dumesic, J. Chem. Phys. 114 (2001) 4663.
[72] R.M. Watwe, Ph.D. thesis, University of Wisconsin-Madison, Madison, WI (2000).